

**FABRICATION AND PERFORMANCE
CHARACTERIZATION OF PET/ITO/ZNO
NANOROD/P3HT:PCBM AND
PET/ITO/P3HT:PCBM SOLAR CELL**

IZZATI HUSNA BINTI ISMAIL

UNIVERSITI SAINS MALAYSIA

2015

**FABRICATION AND PERFORMANCE
CHARACTERIZATION OF PET/ITO/ZNO
NANOROD/P3HT:PCBM AND
PET/ITO/P3HT:PCBM SOLAR CELL**

by

IZZATI HUSNA BINTI ISMAIL

**Thesis submitted in fulfilment of the requirements
for the degree of Master of Science**

ACKNOWLEDGEMENT

First of all, I would like to express my thanks to my main supervisor, Professor Kamarulazizi bin Ibrahim for his excellent guidance and concern throughout the entire research. Secondly, I would like to acknowledge my co-supervisor, Dr. Melati binti Khairuddean from School of Chemistry who offered me the opportunity to boost and improve my knowledge in the field of organic polymer material.

I feel greatly thankful to the entire lab assistant in NOR laboratory for their contribution and support all the time in my research studies. Additionally, I'm indebted and thankful to the USM for offering me USM scholarship to ease my financial burden during my research study. Last but not least, I would like to thank my beloved family and friends for giving me the motivation and inspiration to complete my research study.

TABLE OF CONTENTS

	PAGE
ACKNOWLEDGEMENT	ii
TABLE OF CONTENTS	iii
LIST OF FIGURES	vii
LIST OF TABLE	x
LIST OF SYMBOL	xi
LIST OF ABBREVIATIONS	xiii
ABSTRAK	xiv
ABSTRACT	xvi
CHAPTER 1: INTRODUCTION	
1.1 Background of study	1
1.2 Problem Statement	3
1.3 Objectives	3
1.4 Originality of the research work	4
1.5 Thesis outline	4
CHAPTER 2: LITERATURE REVIEW	
2.1 The history of solar cells - from inorganic to organic	6
2.2 Comparison between generations of solar cell	9
2.3 Basic working principle of organic photovoltaic	9
2.4 Bulk heterojunction and hybrid (ordered) heterojunction solar cell architectures	13

2.4.1	Bulk heterojunction	13
2.4.2	Ordered heterojunction (hybrid)	14
2.5	Poly(3-hexylthiophene) (P3HT)	16
2.6	Electron-acceptor material	17
2.6.1	Methanofullerene Phenyl-C61-Butyric-Acid-Methyl-Ester (PCBM)	17
2.6.2	Zinc Oxide (ZnO) nanorod	18
2.7	Buffer layer	18
2.7.1	PEDOT:PSS	18

CHAPTER 3: METHODOLOGY

3.1	Materials	20
3.2	Instrument and characterization	20
3.2.1	Nuclear Magnetic Resonance (NMR) Spectroscopy	21
3.2.2	Fourier Transfer Infrared (FTIR)	22
3.2.3	Ultraviolet-visible (UV-VIS) spectrophotometer	23
3.2.4	Field Emission Scanning Electron Microscope (FESEM)	24
3.2.5	X-Ray Diffraction (XRD)	24
3.2.6	Solar simulator	25
3.2.7	Spin coating	28
3.2.8	Microwave oven	29
3.3	Production procedure	29
3.3.1	Preparation of substrates	29
3.3.2	P3HT synthesis	30
3.3.3	Preparation of bulk heterojunction device (organic solar cell)	31

3.3.4	Preparation of ordered heterojunction device (hybrid solar cell)	32
-------	--	----

CHAPTER 4: RESULTS AND DISCUSSION OF HYBRID SOLAR CELL

4.1	Synthesis and characterization of ZnO nanorod	34
4.1.1	Synthesis of ZnO nanorod	34
4.1.2	FESEM analysis	35
4.1.3	XRD analysis	39
4.1.4	UV-VIS analysis	41
4.2	Characterization of ZnO nanorod/P3HT and ZnO nanorod/P3HT:PCBM	42
4.2.1	FESEM analysis	42
4.2.2	UV-VIS analysis	46
4.2.3	Solar simulator analysis	48

CHAPTER 5: RESULTS AND DISCUSSION OF ORGANIC SOLAR CELL

5.1	Synthesis and Characterization of P3HT	54
5.1.1	FTIR analysis	54
5.1.2	NMR analysis	55
5.1.3	UV-VIS analysis	56
5.2	Characterization of P3HT:PCBM and PEDOT:PSS/P3HT:PCBM	58
5.2.1	FESEM analysis	58
5.2.2	Solar simulator analysis	62

CHAPTER 6: CONCLUSION AND RECOMMENDATION

6.1 Conclusion 68

6.2 Recommendation 70

REFERENCES 71

PUBLICATIONS 80

APPENDIX

LIST OF FIGURE

	PAGE
Fig. 1: The academic publications on OSC from 1980 through 2011. Accessed through the ISI Web of Science.	2
Fig. 2.1: Dissociation of the excitons with generation of charge.	11
Fig. 2.2: Working principle of organic solar cell.	12
Fig. 2.3: Bulk heterojunction schematic.	13
Fig. 2.4: Schematic diagram of ordered heterojunction.	15
Fig. 2.5: Structure of poly(3-hexylthiophene), P3HT.	16
Fig. 2.6: Structure of PCBM.	17
Fig 2.7: The chemical structure of PEDOT:PSS.	19
Fig. 3.1: 300 MHz and 500 MHz NMR instruments.	22
Fig. 3.2: FT-IR instrument.	22
Fig. 3.3: UV-Vis spectrophotometer.	23
Fig. 3.4: FESEM microscope.	24
Fig. 3.5: XRD instrument.	25
Fig. 3.6: Solar simulator instrument.	25
Fig. 3.7: A typical current-voltage characteristic (Schottky diode) of a solar cell in the dark and under illumination.	27
Fig. 3.8: Typical power curve for solar cell.	27
Fig. 3.9: Spin coating instrument.	28
Fig. 3.10: Microwave oven.	29
Fig. 3.11: Ultrasonic bath.	30
Fig. 3.12: Synthesis process of P3HT.	31

Fig. 3.13:	Bulk heterojunction fabrication.	32
Fig. 3.14:	Hybrid heterojunction fabrication.	33
Fig. 4.1:	Morphology of the synthesized ZnO nanorod prepared by microwave irradiation method using different time and irradiation power (magnification 50k).	37
Fig. 4.2:	Ostwald ripening process.	38
Fig. 4.3:	Schematic diagram of the formation process of ZnO nanorod.	39
Fig. 4.4:	XRD graph for ZnO nanorod with different time growth. Power irradiation of 100W: (a) 5 mins (b) 15 mins (c) 30 mins and power irradiation of 550W (d) 5 mins (e) 15 mins (f) 30 mins.	40
Fig. 4.5:	Absorption spectrum of ZnO nanorod with different time dependent and irradiation power.	41
Fig. 4.6:	Morphology of ZnO nanorod/P3HT using different time dependent and irradiation power (magnification 50k).	43
Fig. 4.7:	Morphology of ZnO nanorod/P3HT:PCBM using different time dependent and irradiation power (magnification 50k).	45
Fig. 4.8:	UV-Vis spectrum of ZnO nanorod/P3HT and ZnO nanorod/P3HT:PCBM using different time dependent and power irradiation of (A) 100 W (B) 550 W.	47
Fig. 4.9:	ZnO nanorod/P3HT with power irradiation of (A) 100 W (B) 550W.	49
Fig. 4.10:	ZnO nanorod/P3HT:PCBM with power irradiation of (A) 100 W (B) 550 W.	51
Fig. 5.1:	Example of organic device.	53
Fig. 5.2:	Black solid of P3HT.	54

Fig. 5.3:	FTIR spectrum of P3HT.	55
Fig. 5.4:	UV-VIS absorption spectra of P3HT, PCBM and different blends of P3HT:PCBM.	57
Fig. 5.5:	Solution (A) P3HT and ratios of P3HT:PCBM (B) 1:0.5 (C) 1:1 (D) 1:4.	58
Fig. 5.6:	FESEM of ITO/P3HT:PCBM thin film with different ratio and thermal annealing.	59
Fig. 5.7:	PEDOT:PSS/P3HT:PCBM with different ratio and thermal annealing.	61
Fig. 5.8:	P3HT:PCBM (A) room temperature (B) 140°C.	62
Fig. 5.9:	PEDOT:PSS/P3HT:PCBM (A) room temperature (B) 140°C.	65
Fig. 5.10:	Comparison between organic and hybrid solar cell efficiency.	67

LIST OF TABLE

	PAGE
Table 3.1: Materials for organic and hybrid solar cell fabrication.	20
Table 3.2: Characterization instruments.	21
Table 3.3: Different temperature annealing and ratio concentration.	31
Table 3.4: Parameter for ZnO nanorod growth.	33
Table 4.1: Diameter and length of ZnO nanorod with different time of growth and power.	35
Table 4.2: Energy gap of ZnO nanorod with different time of growth and power.	42
Table 4.3: Summary of performance for device based on ZnO nanorod/P3HT.	50
Table 4.4: Summary of performance for device based on ZnO nanorod/P3HT:PCBM.	52
Table 5.1: Electrical performance P3HT:PCBM with different in ratio and temperature.	64
Table 5.2: Electrical performance of PEDOT:PSS/P3HT:PCBM with different ratio and temperature.	66

LIST OF ABBREVIATIONS

3HT	3-Hexylthiophene
Al	Aluminium
CDCl ₃	Deuterated chloroform
CHCl ₃	Chloroform
CH ₃ OH	Methanol
FeCl ₃	Anhydrous iron (III) chloride
FESEM	Field emission scanning electron microscope
FTIR	Fourier transfer infrared
HCl	Hydrochloric acid
HMT	Hexamethylenetetramine
HOMO	Highest occupied molecular orbital
HTL	Hole transporting layer
ITO	Indium tin oxide
IV	Current-voltage
LUMO	Lowest occupied molecular orbital
NaOH	Sodium hydroxide
NMR	Nuclear magnetic resonance spectroscopy
OLED	Organic light emitting diode
OSC	Organic solar cell
P3HT	Poly(3-hexylthiophene)
PCBM	Methanofullerene phenyl-C61-butryic-acid-methyl-ester
PEDOT:PSS	Poly(3,4-ethylenedioxythiophene):poly-(styrenesulfonate)
PET	Polyethylene terephthalate

PV	Photovoltaic
Si	Silicon
UV-VIS	Ultraviolet-visible spectrophotometer
XRD	X-Ray diffraction
$\text{Zn}(\text{CH}_3\text{COO})_2 \cdot 2\text{H}_2\text{O}$	Zinc acetate dehydrate
ZnO	Zinc oxide
$\text{ZnO}(\text{NO}_3)_2$	Zinc nitrate hexahydrate

LIST OF SYMBOL

θ	Angle between the sample surface and incident beam
η	Efficiency
π	Integer
d	Inter-planar spacing in the crystal lattice
Δ	Path difference
λ	Wavelength
FF	Fill factor
I_{\max}	Maximum current
I_{sc}	Short circuit current
P_{in}	Power input
P_{\max}	Maximum power
V_{\max}	Maximum voltage
V_{oc}	Open circuit voltage

FABRIKASI DAN PRESTASI PENCIRIAN SEL SURIA PET/ITO/NANOROD ZNO/P3HT:PCBM DAN PET/ITO/P3HT:PCBM

ABSTRAK

Kerja ini memberi tumpuan kepada fabrikasi dan prestasi pencirian sel suria hibrid (NANOROD ZnO/P3HT:PCBM) dan sel suria organik (P3HT:PCBM). Bagi sel suria hibrid, bahan seperti regioregular 3 - hexylthiophene - 2 , 5 – diyl (P3HT) (bahan penderma), zink oksida (bahan penerima) dan fullerene [6,6] phenyl C61 acid butyric methyl ester (PCBM) (bahan penerima) telah digunakan. Sintesis dengan menggunakan kaedah penyinaran gelombang mikro adalah untuk mendapatkan nanorod ZnO. Parameter seperti masa dan kuasa penyinaran akan menyebabkan pertumbuhan yang berbeza dari segi kepanjangan dan diameter, tetapi untuk substrat yang mempunyai/tidak mempunyai lapisan PCBM akan menghasilkan perbezaan kecekapan. Gabungan lapisan antara nanorod ZnO/P3HT:PCBM mempunyai kecekapan yang paling tinggi iaitu 0.39% (kuasa penyinaran 550W, masa sebanyak 30 min dan penambahan PCBM) berbanding dengan gabungan lapisan ZnO/P3HT dengan kecekapan yang hanya 0.17% (kuasa penyinaran 550W, masa sebanyak 30 min dan tiada penambahan PCBM). Selepas itu, untuk sel suria organik bahan seperti P3HT (bahan penderma), PCBM (bahan penerima) dan Poly(3,4-ethylenedioxythiophene) poly (styrenesulfonate) (PEDOT:PSS) (lapisan penimbal) telah digunakan. Kaedah sintesis pengoksidaan pempolimeran digunakan untuk mendapatkan bahan P3HT. parameter seperti suhu, nisbah PCBM dan mempunyai/tidak mempunyai lapisan PEDOT:PSS akan menghasilkan perbezaan kecekapan. Gabungan lapisan PEDOT:PSS/P3HT:PCM mempunyai kecekapan

paling tinggi iaitu 2.44% (nisbah PCBM 1:4, suhu 140°C dan penambahan lapisan PEDOT:PSS) berbanding dengan gabungan lapisan P3HT:PCBM yang hanya mempunyai kecekapan 1.05% (nisbah PCBM 1:4, suhu 140°C dan tiada penambahan lapisan PEDOT:PSS). Kesimpulan yang boleh dibuat dari kerja ini adalah, sel suria organik mempunyai kecekapan yang lebih tinggi berbanding dengan sel suria hibrid.

FABRICATION AND PERFORMANCE CHARACTERIZATION OF PET/ITO/ZNO NANOROD/P3HT:PCBM AND PET/ITO/P3HT:PCBM SOLAR CELL

ABSTRACT

This work focus on the fabrication and performance characterization of hybrid (ZnO nanorod/P3HT:PCBM) and organic solar cell (P3HT:PCBM). For hybrid solar cell, material such as regioregular 3 - hexylthiophene - 2 , 5 – diyl (P3HT) (donor material), zinc oxide (ZnO) (acceptor material) and fullerene [6,6] phenyl C61 acid butyric methyl ester (PCBM) (acceptor material) was used. Synthesis by microwave irradiation method was to get ZnO nanorod. Parameters such as time and irradiation power cause different length and diameter of ZnO nanorod growth, but for substrate with/without PCBM layer yield different efficiency. The combination layer of ZnO nanorod/P3HT:PCBM have highest efficiency of 0.39% (power irradiation 550W, time for 30 mins and with addition of PCBM) compared to the combination layer of ZnO/P3HT with efficiency of only 0.17% (power irradiation 550W, time for 30 mins and without addition of PCBM). After that, for organic solar cell material such as P3HT (donor material), PCBM (acceptor material) and Poly(3,4-ethylenedioxythiophene) poly (styrenesulfonate) (PEDOT:PSS) (buffer layer) was used. Oxidative polymerization synthesis method was used to get P3HT material. Parameters such as temperature, ratio of PCBM and with/without PEDOT:PSS layer yield different efficiency. The combination layer of PEDOT:PSS/P3HT:PCM have highest efficiency of 2.44% (ratio of PCBM 1:4, temperature 140°C and with addition layer of PEDOT:PSS) compared to the

combination layer of P3HT:PCBM with efficiency of only 1.05% (ratio of PCBM 1:4, temperature 140°C and without addition layer of PEDOT:PSS). From these work, it can be concluded that organic solar cell have higher efficiency compared to hybrid solar cell.

CHAPTER 1

INTRODUCTION

1.1 Background of study

Energy consumption is a necessity for human need and the demand is increasing in the recent decades. However, the energy sources (coal, oil and natural gas) are limited which resulted in the search for alternative energy resources such as wind power, wave power, geothermal power and solar power as renewable energy sources. The most promising energy available today is solar power which can be directly converted to electricity.

Nowdays, the highest efficiencies of solar cell using silicon base is 25.6%, by Panasonic (Martin et al., 2014). However, this type of solar cell is limited by its high power conversion cost (Wohrle & Missner, 1991). To solve this problem, solar cell using organic polymer or small organic molecules has been introduced (Tang, 1986). The organic polymer material offers several advantages; material is environmental friendly which can be fabricated by spin-coating, ink-jet printing and roll-to-roll process to reduce the production cost (Saricifti, 2004). These organic polymers are flexible and their physical properties can be tuned (Saricifti, 2004). The photosynthesis in plant uses molecular system to harvest light and convert it into useful chemical energy. This phenomenon inspired the use of organic molecules as light absorbing materials, making the organic solar cell potentially cheap with sustainable technology processing.

This area continues to grow every year. Fig. 1 shows the increasing growth in the number of academic publications on Organic Solar Cell (OSC) over the past 25 years. Several companies worldwide began to commercialize the OSC device in the past decade, which demonstrated a successful mass production of OSC device in the range of 7-10 %, and it was estimated that OSC will make a significant market breakthrough (Martin et al., 2014) when the efficiencies reaches 15 %. The success of commercialized organic light-emitting diodes (OLED) showed that the OSC technology will also follow the similar path, with the ongoing research every year.

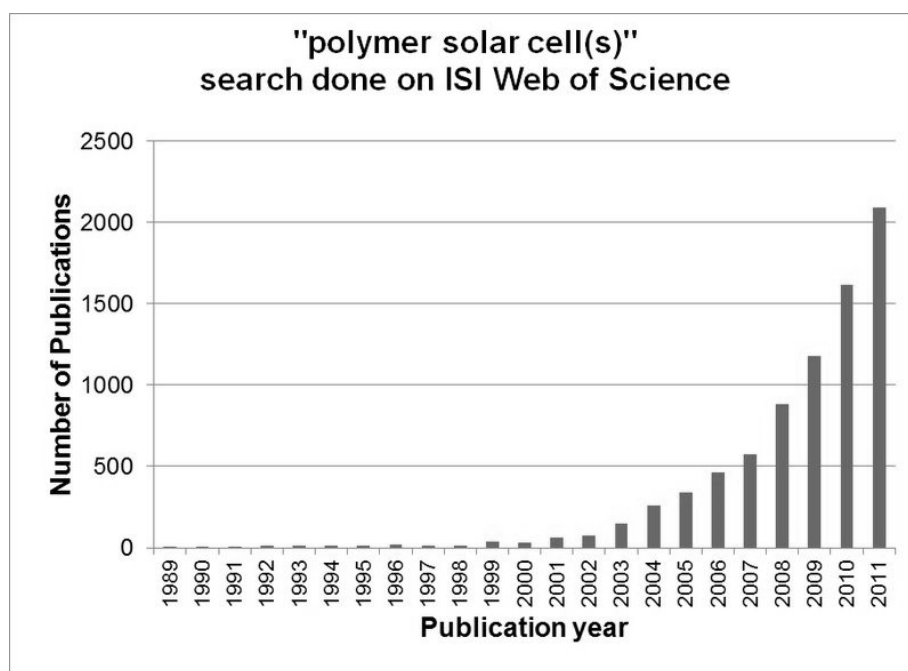


Fig. 1: The academic publications on OSC from 1989 through 2011. (Accessed: ISI Web of Science).

Nowdays, the research work in this field focused on the conducting polymer materials used in solar cell devices. Conducting polymers are conjugated polymers with five-membered heterocyclic compounds. These polymers are common materials in OSC device which exhibited excellent electrical conductivity. The applications

include charging storage devices (batteries, capacitors), sensors, membranes, corrosion protective coatings and photovoltaic device.

1.2 Problem statement

The characteristic of inorganic materials and silicon as substrates in fabrication of highly efficient solar cell are impressive but the processing cost is high. On the other hand, the usage of organic polymers and flexible substrates involved inexpensive process. These materials have their own characteristics such as high electrical conductivity of polythiophene, high electron affinity of PCBM and good hole transporting layer (HTL) material of PEDOT:PSS. Improvements have been done to enhance the efficiency of the organic solar cell. In order to improve the charge transportation, PEDOT:PSS were used as buffer layer before the active layer coating. For improvement on the interpenetrating network between p type and n type materials, bulk heterojunction structures were used instead of the hybrid heterojunction or pn junction.

1.3 Objectives

The main objective of this work is to produce organic solar cell devices which are better than the hybrid solar cell devices. The objectives include:

- To synthesize and characterize P3HT (organic material) using the oxidative polymerization method.
- To synthesize and characterize ZnO nanorod (inorganic material) using microwave irradiation method.

- To fabricate and characterize the device of hybrid solar cell (PET/ITO/ZnO nanorod/P3HT) at different growth time, different microwave power and with/without PCBM.
- To fabricate and characterize the device of organic solar cell (PET/ITO/P3HT:PCBM/Al) with different PCBM ratio, different thermal annealing temperature and with/without PEDOT:PSS.
- Comparison of efficiencies (electrical properties) between hybrid and organic solar cell using solar simulator.

1.4 Originality of the research work

Common traditional solar cell devices used silicon or glass as substrates but they are expensive, not flexible and difficult to handle. This research work focused on the preparation of solar cell devices using flexible substrates (PET), which are lightweight, conformable to non-planar structure with longer lifetime and involved cheap processing.

1.5 Thesis Outline

Chapter 1 consisted of the background study, followed by the problem statement encountered in this research field. Few solutions to overcome the problem were listed in the research objectives which highlighted the preparation of new materials and the study of its efficiency.

Chapter 2 explained the history of solar cell, differentiating between the hybrid and organic solar cells, Some of the important aspects such as the working

principle of these solar cells and the type of architecture for both materials (PEDOT:PSS, P3HT, PCBM and ZnO) were highlighted.

Chapter 3 discussed about the general principles of the characterization instruments which were used and the experimental details for each characterization work.

Chapter 4 focused on the results obtained and the discussion which include data interpretation and the physical and chemical properties of the materials, ZnO nanorod/P3HT. The work focused on the different growth time, different microwave power and with/without PCBM solution.

Chapter 5 discussed different material of P3HT:PCBM with different ratio of PCBM, different thermal annealing temperature and with/without PEDOT:PSS layer.

Chapter 6 concluded the overall discussion of the study, meeting all the mentioned work in the objectives listed earlier in Chapter 1. Some recommended work for future study were also suggested.

CHAPTER 2

LITERATURE REVIEW

2.1 The history of solar cells – from inorganic to organic

The photovoltaic effect is the basic physical process through which a solar cell converts sunlight into electricity. In 1839, Edmund Becquerel, discovered the photovoltaic effect while experimenting with an electrolytic cell made up of two metal electrodes (Becquerel et al., 1939). Charles Fritts created the first working selenium cell in 1883, where he coated the semiconductor material selenium with a very thin layer of gold (Borisenko et al., 2008). The resulting cells showed only 1 % of the conversion of electrical efficiency, which might be due to the host cost of selenium, preventing such cells for energy supply. The development of the solar cell technology continued where in 1941, Russell Ohl created the silicon p-n junction cells with efficiencies above 5 %, followed by the discovery of the first practical solar cell at Bell laboratory in 1954, where Chapin, Fuller and Pearson created a cell based on a silicon p-n junction with 6 % power conversion efficiency. Today's best silicon solar cells have over 40 % efficient, with the industrial average of over 17 % (Chapin et al., 1954).

The existing photovoltaic nowadays still followed the first generation Si-base cell, although much improvement has been made in terms of efficiency and stability of the devices. The usage of tandem cell structure has been introduced to capture as many incident photons as possible, which led to the increased efficiency up to 40.8 %

(Geisz et al., 2008). Solar cells using a very complex structure based on crystalline Si and/or other inorganic semiconductor with higher efficiencies of 41.7 was developed at the Fraunhofer Institute in Freiburg (Fraunhofer ISE., 2009). The solar cell industry is still dominated by the first generation solar cell based on Si wafer, which covers about 90 % of the world market (Tao et al., 2008). However, the efficiency of these commercialized Si based solar cells is between 14-19 %, which is much lower than the one previously reported (Schultz et al., 2007). Increased cost of production is needed to improve the efficiencies of the solar cells.

Solar cell efficiency can be achieved using the conventional inorganic photovoltaic, but such technology to be used as household energy source involves very high cost, approximately five times higher than the electricity obtained from fossil fuels (Tao et al., 2008). This technology is very expensive because it requires high cost of materials and fabrication processes. However, the cost of manufacturing solar cells can be reduced by decreasing the amount of Si (thinner Si wafer), or by replacing with other suitable materials such as cadmium telluride (CdTe) or copper indium gallium selenide (CIGS) (Tao et al., 2008). These types of solar cells belong to the second generation of photovoltaic, where fabrication and production costs are lower than the first generation devices but with efficiencies in the range of 9-12 % (Hegedus et al., 2006), or around 30 % with tandem cell architecture device (Dimroth et al., 2006).

In the past 30 years, the third generation solar cell has been increasingly improved. This type of devices, which include dye synthesized solar cell (DSSC), organic small molecules, polymeric solar cells and nanocrystal solar cells have been

widely developed. The third generation solar cells differ from the first and second generations in terms of the traditional p-n junction to separate the photogenerated charge carriers. Solar cells today are used in all sorts of devices, from calculators to rooftop solar panels. Improved designs and advanced materials have made it possible to build solar cells that reach over 40 % efficiency. Research and development continues in this area to bring down the cost and to raise the percentage of efficiency so that solar power will be more competitive with fossil fuels.

OSC have been developed for more than three decades but only in the last decade the research was extensively explored (Chamberlain et al., 1983). Introduction of new materials and sophisticated device structures created a rapid increase in power conversion efficiencies which has attracted scientific and economic interest. It was reported that the highest efficiency OSC has reached 10.7 % (Martin et al., 2014) but it still cannot compete with the inorganic photovoltaic device. The huge advantages of OSC device compared to the Si-base cells are light weight, flexible, variety of fabrication process, low cost material for mass production and capable to change the energy band gaps of materials via molecular design, synthesis, and processing (Sun et al., 2005).

One of the strategies to increase the efficiency of the OSC device is to use the hybrid and bulk heterojunction architecture. The limitations when using hybrid and bulk structure include poor charge carrier mobility and narrow overlapping of the absorption spectra of the organics with the solar spectrum (Ameri et al., 2009). Although organic solar cell has improved, its lifetime performance and degradation of OSC device are still at the early stage (Hauch et al., 2008).

2.2 Comparison between generations of solar cell

- **1st and 2nd generation solar cells :**

Base: silicon or glass; Active layer: CdSe, GaN, ZnO and etc.

Disadvantage: high cost process leads to expensive materials and not flexible.

- **3rd generation solar cells :**

Base: mostly use glass; Active layer: organic materials

Disadvantage: even though it involves low cost process but still it is not flexible.

2.3 Basic working principles of organic photovoltaic

Organic materials can transport electric current and absorb light in the ultraviolet (UV) visible part of the solar spectrum due to their delocalized π conjugation. The charge mobility of organic materials is lower than inorganic material. However, this can be balanced with the strong absorption coefficients (typically $\geq 10^5 \text{ cm}^{-1}$), which allow high absorption in $\leq 100 \text{ nm}$ thick devices. Furthermore, the light absorption (primary photoexcitation) in inorganic materials generates free charges which are separated at the junction while in organic materials, the photoexcitation in the active layer are electron-hole pairs called excitons. The excitons are neutral excited states, with typical binding energy from 0.05 to $> 1 \text{ eV}$. The exciton diffusion length for organic solar cell device is usually in the range of 5 to 15 nm (Stubinger et al., 2001).

The process of converting light into electricity by means of organic solar cells takes place through intermediate charge separated states called geminates pairs, which are fundamental intermediates in the photoconversion process. Strong electric fields are applied in order to be separated into free charge carriers (Hoppe et al.,

2004). The process for organic solar cell device is described in the following steps below:

Step 1: Absorption of light and generation of excitons

When the electron donor material is illuminated, electron will occupy the HOMO orbital and will be absorbed. The electron will be excited into the LUMO orbital of the donor material and created a strong bound electron-hole pair called exciton.

Step 2: Diffusion of excitons to an active interface

In order to generate a current, the exciton has to reach the interface of the electron donor and acceptor materials during its lifetime. A significant difference between organic and inorganic solar cells lies in the structure of the cell. Organic materials are amorphous and disordered, which makes the charge transport much more difficult compared to the crystalline cells structure. Exciton with high diffusion coefficient have a longer lifetime and can travel longer distance before the exciton decayed to the ground state, which produced heat, vibration or released photons from the absorption. The balance between the exciton diffusion lengths, film thickness and exciton lifetime were considered when fabricating an organic solar cell. A promising cell design is the bulk heterojunction solar cell architecture.

Step 3: Dissociation of the excitons with generation of charge

Since the exciton binding energies are relatively high ($0.5 > 1$ eV), the build in electric fields of the orders of 10^6 - 10^7 V/m are not high enough to separate the exciton directly, but the separation of the exciton into charge carriers can be achieved at the interface of the electron donor/acceptor material by the sharp drop of potential

(Hoppe et al., 2004). Fig. 2.1 shows the process of the exciton at the interface of the electron donor (D) and electron acceptor (A) materials. The ground state of the two materials is the lowest energy state. It is assumed that the exciton is produced in the donor component, labeled as D^* (excited state in the donor). When the exciton reaches the interface, with the state and energy correspond to the exciton energy (D^*), the exciton will transfer its electron to the acceptor material and the hole remains on the polymer chains from the donor material. This creates the charge transfer state (D^+A^-) in which the electron (negative charge) and a hole (positive charge) will move away from each other, resulting in a charge separated state. To produce an electric current, a full charge separation of the electron and hole has to occur. One of the main reasons for low cell efficiency is the recombination of electron and hole (K_{CR}) in the charge transfer state (CT state), resulting in an efficiency loss. To maximize the efficiency, the rates of charge transfer (K_{CT}) and charge separation (K_{CS}) have to be increased. Furthermore the rate of charge recombination (K_{CR}) has to be reduced (Hoppe et al., 2004).

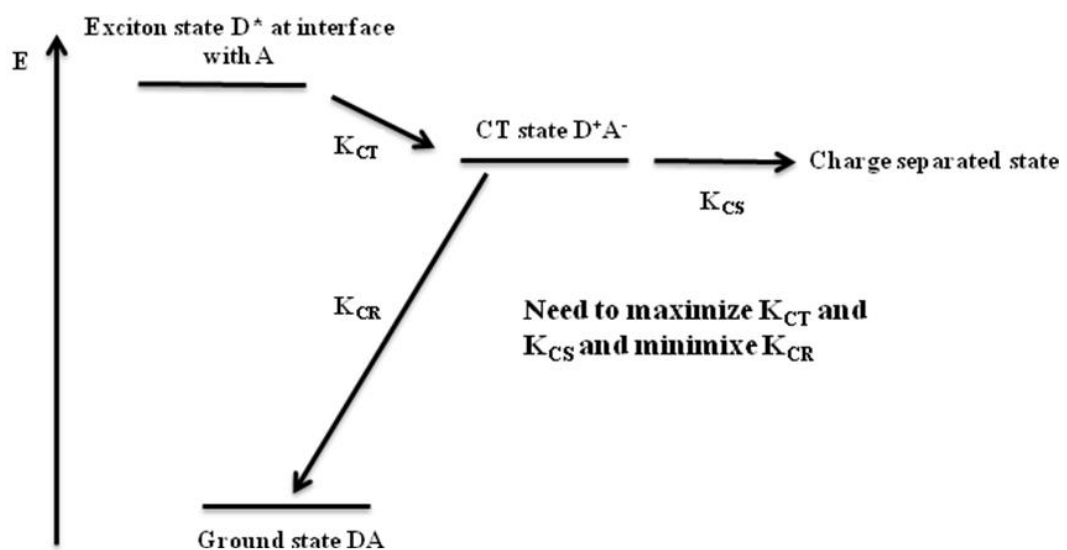


Fig. 2.1: Dissociation of the excitons with generation of charge (Hoppe et al., 2004).

Step 4: Charge transport and charge collection

It usually takes a strong electric field to separate an exciton into free charge carriers because of the high exciton binding energy. After the separation of the electron and hole, electric field created will push the separated free charge carriers towards the electrode. The electron will be drifting towards the cathode and the hole will drift to the anode. The charge carrier mobility in organic semiconductor is lower than inorganic semiconductor. This has a large effect on the efficiency and design of the organic solar cells. If the organic material in the solar cell is more ordered, the mobility of the charge carriers will increased, resulting in faster electron and hole separation because they can move very fast, to be away from each other. The charge carriers are collected at the electrodes (Fig 2.2) and if the electrical circuit is connected to the electrodes an electrical current will flow through (Hoppe et al., 2004).

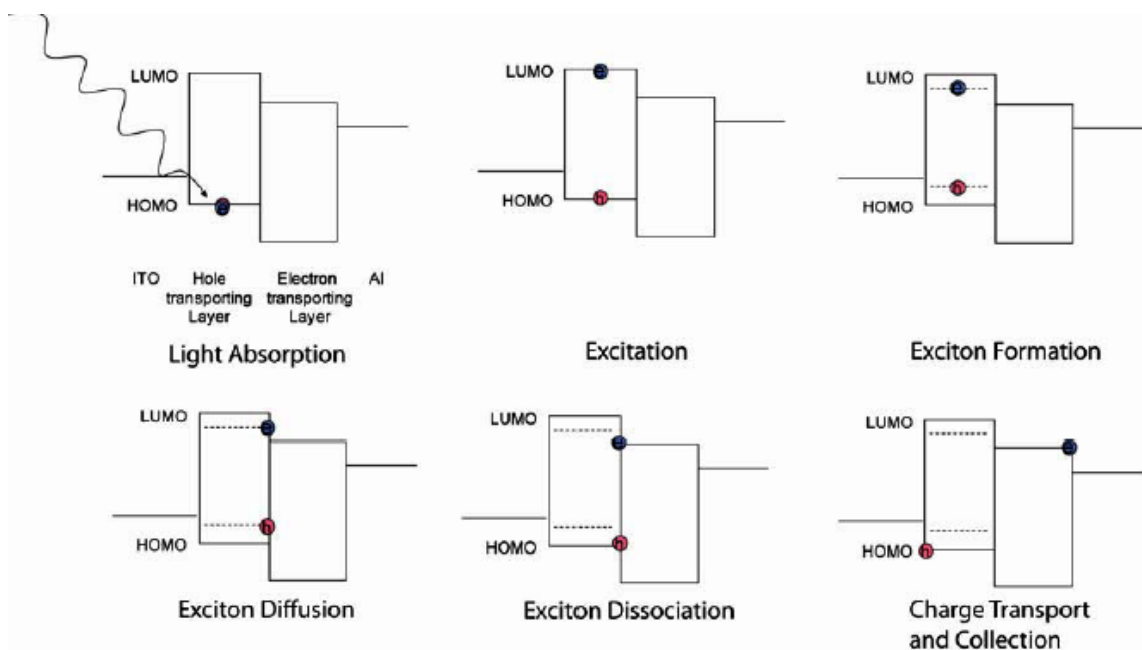


Fig. 2.2: Working principle of organic solar cell (Hoppe et al., 2004).

2.4 Bulk heterojunction and hybrid (ordered) heterojunction solar cell architectures.

The difference between organic and hybrid heterojunction device lies in the exciton dissociation process, where this process occurs at different location in the active layer. In this section, the most investigated device structure will be described, which are bulk heterojunction and hybrid (ordered) architectures.

2.4.1 Bulk heterojunction

In the bilayer heterojunction, donor and acceptor are completely separated into p-type and n-type layers but in the bulk heterojunction architecture both p-type and n-type layers are mixed together to form an interpenetrating network, as shown in Fig. 2.3. As a result, the active surface area of the interface increased and the excitons can dissociate whenever they are created within the bulk (Yu et al., 1995). Two-dimensional interface of the bilayer approach is exchanged by a three-dimensional interpenetrating network.

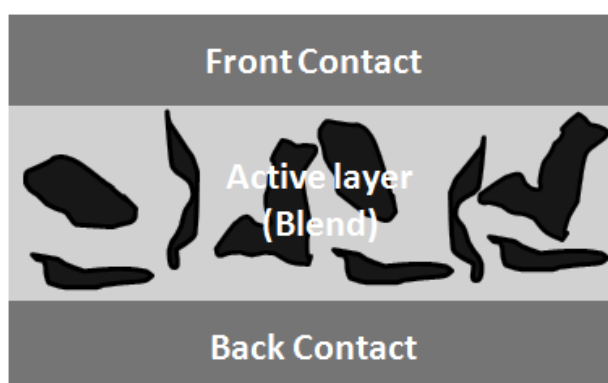


Fig. 2.3: Bulk heterojunction schematic.

In 1995, the bulk heterojunction solar cell architecture was first reported, with efficiency below 1 %. Later, the researcher interest focused on the bulk

heterojunction architecture type, whereby the number of publications in this field increased. The highest efficiency reported for the bulk heterojunction type was 10.7 % (Martin et al., 2014). The huge interest on the bulk heterojunction solar cells arose from a reasonably high efficiency, cheap and easy fabrication technology. In fact, it can be prepared by solution processing technique, such as spin coating, screen printing, inkjet printing and spray coating (Ishikawa et al., 2004). However, even if the preparation of bulk heterojunction is rather simple, mechanism and the operation principles are complex and not completely clarified yet.

2.4.2 Ordered heterojunction (Hybrid)

Most of the bulk heterojunction solar cells were made by mixed semiconductor materials, such as polymer-polymer, polymer-fullerene derivative or polymer-nanocrystal to make blends. Although this type of architecture device is easy to fabricate by using simple process to manufacture the solar cell, there were problems encountered within the disordered nanostructure. In some cases, two semiconductor phases were separated with huge length scale, making the excitons not able to make it to an interface to be split by the electron transfer before it decayed. In other cases, one of the phase contained dead ends or islands that prevented the charge carriers from reaching the electrodes.

Ordered bulk heterostructure solar cells, shown in Fig. 2.4, are harder to fabricate compared to the disordered blends. The dimensions of both phases can be controlled to make sure that every spot in the film is within an exciton diffusion length of the interface, between the two semiconductor layers. Using hybrid heterojunction structure gave the electrons and holes the ordered pathways to the

electrodes, after excitons are splitted by the electron transfer. This type of structure allows the carrier to escape from devices as quickly as possible, which then minimized the recombination and showed the possibility to align the conjugated polymer chains and increased the mobility of the charge carrier (Kevin et al., 2005). Nevertheless, hybrid structure is easier to model and understand. However, this type of device structure has problem regarding the diameter and length of the nanostructure. If the length and diameter are not optimized correctly, the solution will not infiltrate well between the nanostructures and the efficiency will immediately decrease.

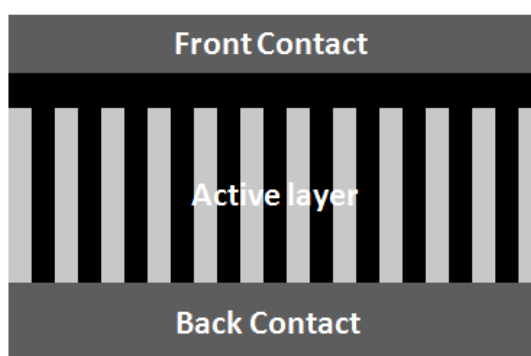


Fig. 2.4 Schematic diagram of ordered heterojunction.

The first hybrid heterojunction containing CdS or CdSe nanoparticle and infiltrated with MEH-PPV was reported by Greenham group (Greenham et al., 1996). One of the most studied material systems among the nanocrystal-polymer blends is zinc oxide (ZnO), in combination with MDMO-PPV or P3HT. Beek (2004) presented the first polymer solar cells containing ZnO nanoparticles with power conversion efficiencies of 1.67 % (Beek et al. 2004).

2.5 Poly(3-hexylthiophene) (P3HT)

Polythiophene types are the most common conducting polymers used in organic solar cell applications with intrinsic conductivity arose from the extended and delocalized π conjugation (Chandrasekhar, 1999). Conducting polymers usually contain simple heteroatoms, such as N and S (in addition to the usual C and H). The conductivity was achieved by chemical or electrochemical oxidations or reactions, or by introduction of dopants, such as the anionic or cationic species. The polymer backbones need to be oxidized or reduced to introduce the charge carriers for conductivity. Conjugated polymers were charged as a consequence of a photoinduced electron transfer reaction. Poly(3-hexylthiophene), P3HT, as shown in Fig. 2.5, is an electron donor material, because of its excellent charge transport properties. Moreover, it absorbed in a wide range of visible region, between 400 and 650 nm (Vanlaeke et al., 2006), with the absorption edge around 650 nm, close to the sun's maximum photon flux (650-700 nm). There are five different methods to synthesize P3HT which are polymerization of thiophene monomers with FeCl_3 (Pomerantz et al., 1991), Yamamoto polymerization (Yamamoto et al., 1992), McCullough method (McCullough et al., 1993), Rieke-Zinc (Zn^*)-Mediated polymerization (Chen et al., 1995) and Rieke-Nickel-Catalyzed Polymerization (Pomerantz et al., 1999).

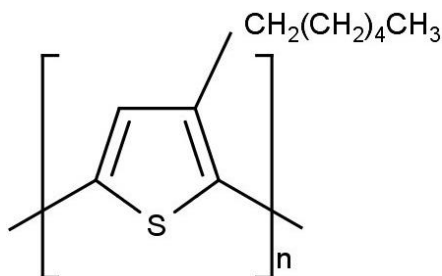


Fig. 2.5: Structure of poly(3-hexylthiophene), P3HT (Pomerantz et al., 1991).

2.6 Electron-acceptor materials

2.6.1 Methanofullerene Phenyl-C61-Butyric-Acid-Methyl-Ester (PCBM)

During these past few years, fullerene organic acceptor was widely used due to its high efficiency solar cell. Fullerene was first discovered in 1985 by Kroto, Curl and Smelly (Kroto et al., 1985) who received the Nobel Prize in Chemistry in 1996. Fullerenes can be chemically modified to improve the solubility of the solution in organic solar cell. Soluble fullerene derivatives are known as some of the best n-type semiconductors. PCBM, one of the best processable n-type semiconductor which can be blended with p-type conjugated polymer to make the photovoltaic cells and thin film organic field effect transistor (OFETs). Methanofullerene Phenyl-C61-Butyric-Acid-Methyl-Ester (PCBM) substituted in C_{60} was first synthesized by Wuld group (Wuld, 1995). The chemical structure of fullerene is shown in Fig. 2.6. This material has high electron affinity, good conductivity and large band gap of ~ 2.3 eV. PCBM is highly soluble in chlorobenzene, toluene, chloroform and other organic solvents, making it suitable for solution-based processing methods such as spin coating. PCBM has the energy levels of -6.1 eV for the HOMO and -3.8 eV for the LUMO (Meijer et al., 2003).

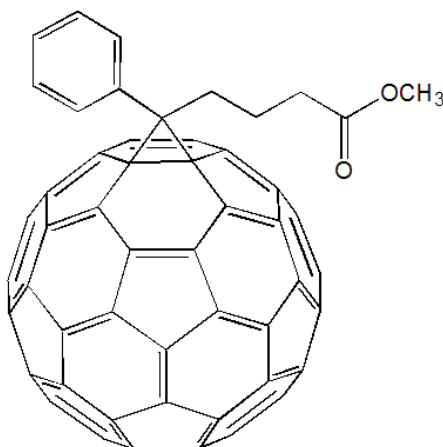


Fig. 2.6: Structure of PCBM (Kroto et al., 1985).

2.6.2 Zinc Oxide (ZnO) nanorod

One-dimensional (1D) nanoscale materials such as nanowires, nanotubes and nanorods with excellent properties and functionalities, have been used as building blocks of nanoscale electronic and optoelectronic devices (Morales et al., 1998). Nowadays, zinc oxide (ZnO) is the most nanoscale material which has been used with a wide band gap of n-type semiconductor (3.37 eV). It has large exciton binding energy of 60 meV at room temperature and also absorbance in the UV range. In addition, ZnO has strong piezoelectric and pyroelectric properties with high electron affinity, allowing it to match with the LUMO of almost all organic semiconductor materials (Su et al., 2005). Due to these properties, ZnO have been used in many applications, such as gas sensors, transparent electrodes, pH sensors, biosensors, acoustic wave devices, UV-photodiodes and solar cell (Wang, 2004). Over the years, extensive investigations have focused on the synthesis of nano and microarchitectures using different methods, such as hydrothermal, sol-gel, electrochemical deposition, vapor-phase process and microwave.

2.7 Buffer layer

2.7.1 PEDOT:PSS

Buffer layers between back contact and active layer have been used because they have specific blocking and/or transport properties. P-type buffer layer is the interface between indium tin oxide (ITO) and thin layer of poly(ethylene dioxythiophene), doped with polystyrene sulfonic acid (PEDOT:PSS). PEDOT:PSS layer has been widely used in photovoltaic because it is able to improve the charge transportation. PEDOT:PSS (Fig. 2.7) is a good hole transporting layer (HTL) material, when spin coated on ITO, it smoothes its surface and enhances the adhesion

of the organics onto ITO. PEDOT:PSS is easily degraded under UV illumination. Moreover, due to the highly hygroscopic nature of PEDOT:PSS (Huang et al., 2005), it gives water to the organic film. Thermal annealing is important to make sure that the device is stable before coating the active layer. The conductivity of PEDOT:PSS slowly reduces without thermal treatment (Huang et al., 2005).

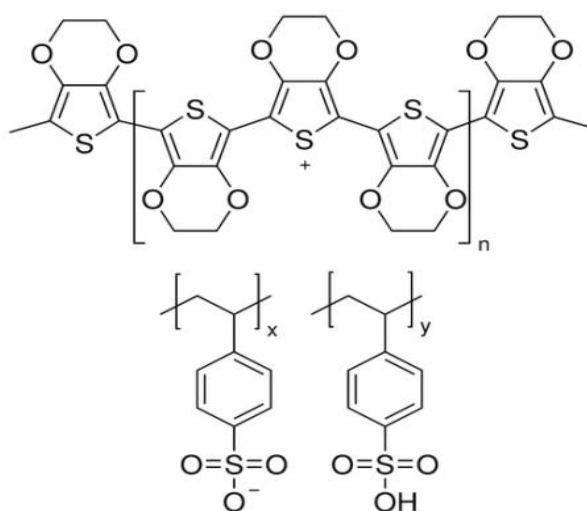


Fig. 2.7: The chemical structure of PEDOT:PSS (Nardes et al., 2007).

PEDOT:PSS has excellent properties as transparent electrode material in organic optoelectronic devices. It has been used as buffer layer and back contact (anode) in photovoltaic devices (Nardes et al., 2007). The ratio of PEDOT:PSS increases with the increasing conductivity. PEDOT:PSS is commercially sold by Heraeus under the trade name Clevios. The formulation of Clevios PH1000 has a ratio of 1:2.5 by weight with conductivity of 1000 S cm^{-1} .

CHAPTER 3

MATERIALS AND METHODOLOGY

3.1 Materials

Table 3.1 represents the materials used for organic and hybrid solar cell fabrication. The materials are as listed in Table 3.1

Table 3.1: Materials for organic and hybrid solar cell fabrication

No	Material
1	3-Hexylthiophene $\geq 99\%$ (3HT)
2	Anhydrous Iron (III) Chloride (FeCl_3)
3	Hydrochloric acid (HCl)
4	Chloroform (CHCl_3)
5	Methanol (CH_3OH)
6	Zinc nitrate hexahydrate $\text{Zn}(\text{NO}_3)_2$
7	Zinc acetate dehydrate $[\text{Zn}(\text{CH}_3\text{COO})_2 \cdot 2\text{H}_2\text{O}]$
8	Sodium hydroxide (NaOH)
9	Hexamethylenetetramine (HMT)
10	[6,6]-Phenyl C61 Butyric Acid Methyl Ester $>99\%$ (PCBM)
11	Poly (3,4-ethylenedioxythiophene) Polystyrene Sulfonate (PEDOT:PSS)

3.2 Instrument and characterization

Table 3.2 shows the summary of instruments used for fabrication and characterization of the materials.

Table 3.2: Characterization instruments

No	Instrument	Model	Function/Characterization
1	Spin Coater	SCS G3P-8	Coat solution on substrate
2	Microwave	Panasonic NN-GD5705	Synthesis ZnO nanorod
3	Fourier Transfer Infrared (FTIR)	Perkin Elmer Spectrum GX	Determine functional groups in the structure
4	Nuclear Magnetic Resonance Spectroscopy (NMR)	Bruker Avance 300 MHz	Confirm the chemical structure
5	Ultraviolet-visible spectrophotometer (UV-VIS)	Cary 5000	Optical properties
6	Field Emission Scanning Electron Microscope (FESEM)	FEINovaNano SEM 450	Morphology, size and thickness
7	X-Ray Diffraction (XRD)	PANalytical X'Pert Pro MRD PW3040	Crystallinity, grain size and orientation
8	Solar simulator	NI PXIE-1073	Electrical properties

3.2.1 Nuclear Magnetic Resonance (NMR) Spectroscopy

NMR spectroscopy is a technique used to determine the molecular structure of a compound for atomic nuclei ^1H and ^{13}C . The NMR (^1H and ^{13}C) spectra were obtained using a Bruker 500 MHz UltrashieldTM spectrometer. 20 mg sample is dissolved in deuterated solvent in an NMR tube. The interpretations of the NMR spectra were recorded by chemical shifts in ppm.



Fig. 3.1: 300 MHz and 500 MHz NMR instruments.

3.2.2 Fourier Transfer Infrared (FTIR)

FT-IR (Fig. 3.2) is a technique used to determine the functional groups in a sample. The absorption band is the characteristic of the chemical bond as can be seen in the spectra. Samples are scanned at range of 700 to 4000 cm^{-1} . All spectra were obtained using Perkin Elmer 2000 FTIR.



Fig. 3.2: FT-IR instrument.

3.2.3 Ultraviolet-visible (UV-VIS) spectrophotometer

UV-VIS spectrophotometer (Fig. 3.3) is used to analyze materials in the ultraviolet-visible region. Infrared spectroscopy depends on vibration motions, but UV-VIS spectroscopy is based on electronic transitions. From UV-VIS spectroscopy, wavelength and absorbance of material can be determined. To determine absorbance of material Beer's Law is being used:

$$A = \epsilon bc \quad (3.1)$$

Where A is absorbance, ϵ is molar extinction coefficient, b is path length and c is concentration. Energy band gap of a material can be determined by using equation:

$$E = \frac{hc}{\lambda} \quad (3.2)$$

Where E is energy, h is Planack's constant, c is speed of light and λ is wavelength.



Fig. 3.3: UV-Vis spectrophotometer.

3.2.4 Field Emission Scanning Electron Microscope (FESEM)

FESEM (Fig. 3.4) is a microscope that works with electron, liberated by field emission source (particle with negative charge) instead of light. FESEM is used to analyze the morphology, size and thickness of devices.



Fig. 3.4: FESEM microscope.

3.2.5 X-Ray Diffraction (XRD)

XRD (Fig. 3.5) is used to analyze crystalline materials to give data of crystalline phase, degree of crystallinity, amount of amorphous content and orientation of crystallites. XRD instrument is using Bragg's diffraction principle which is defined by:

$$n\lambda = 2d \sin \theta = 2\Delta \quad (3.3)$$

Where n is an integer, λ is wavelength, d is the inter-planar spacing in the crystal lattice, θ is the angle between the sample surface and incident beam and Δ represent the path difference.